Quasi-periodic X-ray eruptions and tidal disruption events prefer similar host galaxies

T. WEVERS [ID],[1] K. D. FRENCH [ID],[2] A. I. ZABLUDOFF,[3] T. FISCHER,[4] K. ROWLANDS,[4,5] M. GUOLO,[6] B. DALLA BARBA,[7,8]
R. ARCODIA,[9] M. BERTON,[10] F. BIAN,[10] I. LINIAL [ID],[11,12] G. MINIUTTI,[13] AND D.R. PASHAM [ID][9]

[1] *Space Telescope Science Institute, 3700 San Martin Drive, Baltimore, MD 21218, USA*
[2] *Department of Astronomy, University of Illinois, 1002 W. Green St., Urbana, IL 61801, USA*
[3] *Department of Astronomy and Steward Observatory, University of Arizona, 933 N Cherry Ave, Tucson, AZ 85721, USA*
[4] *AURA for ESA, Space Telescope Science Institute, 3700 San Martin Drive, Baltimore, MD 21218, USA*
[5] *William H. Miller III Department of Physics and Astronomy, Johns Hopkins University, Baltimore, MD 21218, USA*
[6] *Bloomberg Center for Physics and Astronomy, Johns Hopkins University, 3400 N. Charles St., Baltimore, MD 21218, USA*
[7] *Università degli studi dell'Insubria, Via Valleggio 11, Como 22100, Italy*
[8] *Osservatorio Astronomico di Brera, Istituto Nazionale di Astrofisica (INAF), Via E. Bianchi 46, Merate (LC) 23807, Italy*
[9] *MIT Kavli Institute for Astrophysics and Space Research, 70 Vassar Street, Cambridge, MA 02139, USA*
[10] *European Southern Observatory, Alonso de Córdova 3107, Vitacura, Santiago, Chile*
[11] *Institute for Advanced Study, 1 Einstein Drive, Princeton, NJ 08540, USA*
[12] *Department of Physics and Columbia Astrophysics Laboratory, Columbia University, New York, NY 10027, USA*
[13] *Centro de Astrobiología (CAB), CSIC-INTA, Camino Bajo del Castillo s/n, ESAC campus, 28692 Villanueva de la Cañada, Madrid, Spain*

ABSTRACT

In the past five years, six quasi-periodic X-ray eruption (QPE) sources have been discovered in the nuclei of nearby galaxies. Their origin remains an open question. We present MUSE integral field spectroscopy of five QPE host galaxies to characterize their properties. We find that 3/5 galaxies host extended emission line regions (EELRs) up to 10 kpc in size. The EELRs are photo-ionized by a non-stellar continuum, but the current nuclear luminosity is insufficient to power the observed emission lines. The EELRs are decoupled from the stars both kinematically and in projected sky position, and the low velocities and velocity dispersions (< 100 km s^{-1} and $\lesssim 75$ km s^{-1} respectively) are inconsistent with being AGN- or shock-driven. The origin of the EELRs is likely a previous phase of nuclear activity. The QPE host galaxy properties are strikingly similar to those of tidal disruption events (Wevers et al. submitted). The preference for a very short-lived (the typical EELR lifetime is $\sim$15 000 years), gas-rich phase where the nucleus has recently faded significantly suggests that TDEs and QPEs may share a common formation channel, disfavoring AGN accretion disk instabilities as the origin of QPEs. In the assumption that QPEs are related to extreme mass ratio inspiral systems (EMRIs; stellar-mass objects on bound orbits about massive black holes), the high incidence of EELRs and recently faded nuclear activity can be used to aid in the localization of the host galaxies of EMRIs discovered by low frequency gravitational wave observatories.

Keywords: tidal disruption events — accretion disks — black holes

1. INTRODUCTION

Quasi-periodic X-ray eruptions (QPEs) are a recent addition to the various modes of rapid variability observed in massive black holes (MBHs) inhabiting galac-

tic nuclei. Their timing and spectral properties, including quasi-periodic behavior and the emergence of an additional hot thermal component during the outburst rise, are unique among the known variability of active galactic nuclei (AGN; Miniutti et al. 2019; Giustini et al. 2020; Arcodia et al. 2021). QPEs may relate to accretion disk instabilities (Sniegowska et al. 2020; Raj & Nixon 2021; Pan et al. 2023) or to the interaction between the SMBH (or an accretion disk surrounding

Corresponding author: Thomas Wevers
twevers@stsci.edu

it) and a stellar-mass companion. The latter class of models comes in many flavors, including repeated partial tidal disruptions (King 2022), Roche-lobe overflow (Lu & Quataert 2023; Krolik & Linial 2022; Metzger et al. 2022) and star- or BH-disk interactions (Linial & Metzger 2023; Franchini et al. 2023; Tagawa & Haiman 2023; Zhou et al. 2024).

Observationally, several QPEs occur over the course of a long-term (∼years) lightcurve decline, which may be related to the tidal disruptions of stars (Miniutti et al. 2023; Arcodia et al. 2024). Some QPEs also exhibit rebrightening episodes. Other clues that hint at a potential connection between QPEs and tidal disruption events (TDEs) include the discovery of QPE-like flares in TDE candidates (Chakraborty et al. 2021; Quintin et al. 2023). From a theoretical perspective, some models require a compact accretion disk to explain the QPEs, which similarly require a TDE to render the QPEs visible (Linial & Metzger 2023).

Further similarities between QPEs and TDEs can be found in their host galaxies, which have been inferred to contain black holes smaller ($\sim 10^6$ M$_\odot$) than in typical AGNs. Wevers et al. (2022) also noted that QPEs are overrepresented among post-starburst (PSB) and quiescent Balmer strong (QBS) galaxies, which are rare ($\lesssim 0.2$ and 2 per cent, respectively) in the local Universe. TDEs are similarly known to be overrepresented among PSB and QBS galaxies (French et al. 2016; Graur et al. 2018). A recent study of integral field spectroscopy of a large sample of PSB galaxies by French et al. (2023) revealed that of the six sources that have extended emission line regions (EELRs) of ionized gas, one was the host galaxy of a TDE (AT2019azh) and one was host to a QPE (RXJ1301). Evidence for an EELR also exists in *Hubble Space Telescope* (HST) narrow-band imaging of the host galaxy of the QPE GSN069, including a marginally resolved, compact (< 35 pc) component and a larger scale (~ 2 kpc, all throughout the HST field of view) component (Patra et al. 2024).

Based on the presence of line ratios that require a hard, non-stellar continuum in long-slit spectroscopy of the QPE nuclei, Wevers et al. (2022) suggested that a long-lived accretion flow may play an important role in the QPE phenomenon. A study of the spatially resolved properties of the QPE host galaxies can be used to trace their merger and accretion history, which can provide further clues to the importance (or lack thereof) of AGN activity on the rate of nuclear transients such as QPEs and TDEs.

In this work we present MUSE integral field spectroscopy of five QPE host galaxies. We describe the observations and data analysis in Section 2. We present the main results in Section 3, including the presence of extended emission line regions of ionized gas with peculiar kinematics that are decoupled from the stellar motions, and evidence for recently faded AGNs. We discuss these results in the context of the connection between QPEs and TDEs based on their similar host galaxy preferences, as well as implications for the theoretical models invoked to explain QPEs, in Section 4, and present the main conclusions in Section 5.

2. OBSERVATIONS AND ANALYSIS

We used the Multi Unit Spectroscopic Explorer (MUSE, Bacon et al. 2010) instrument mounted on the Very Large Telescope Unit 4 (Yepun) to observe the host galaxies of 5/6 known QPE sources (Miniutti et al. 2019; Giustini et al. 2020; Arcodia et al. 2021, 2024). MUSE integral field observations cover a 1×1 arcmin field of view with a spatial sampling (spaxel size) of 0.2 arcsec. The approximately constant spectral resolution of ≈2.62Å corresponds to a velocity resolution of 80 (160) km s^{-1} in the blue (red) wavelength range. An overview of the basic source properties can be found in Table A1, and a full observing log is provided in Table A2.

Galactic foreground extinction is removed prior to the data analysis in accordance with the E(B–V) values reported by Schlafly & Finkbeiner (2011) as tabulated in Table A1 and assuming R$_V$ = 3.1.

We use pseudo-aperture spectra (with a size equal to the typical PSF FWHM of the observations in Table A2) of the nuclei to study the nuclear stellar properties. We also analyze the individual spaxel data where the signal to noise ratio around 5400 Å is >5, and we create pseudo-aperture spectra in various regions of the extended emission line regions to confirm the results of our spatially resolved analysis with higher SNR.

To analyze the morphology, stellar and ionized gas kinematics and properties we use the penalized pixel fitting routine (PPXF; Cappellari 2023). All quoted line velocity dispersions are corrected for instrumental broadening.

2.1. *Kinematics and line fluxes*

We employ the full MILES single stellar population (SSP) library (Vazdekis et al. 2015) to fit the stellar continuum contribution as a linear combination of SSPs and constrain the stellar kinematics. Regions with strong emission and (telluric) absorption lines (as well as the Na I D doublet) are masked during this process.

Following the determination of the best-fit SSP templates, they are subtracted before analyzing the emission lines. There is no evidence of broad emission lines in the galaxy nuclei (see also Wevers et al. 2022), nor

for multiple kinematic components to the narrow lines (see Figures A4, A5 and A6 for example spectra). We therefore use a single kinematic component, parameterized by a narrow Gaussian, to determine the velocity dispersions, velocities and fluxes of the emission lines on the scale of the native spaxel size. Note that the PSF FWHM is generally much larger (see Table A2), so at the smallest spatial scales these measurements will be correlated. We have verified that decoupling the line widths and velocities for each emission line (or doublet) does not significantly alter the results. Similarly, the stellar continuum subtraction does not significantly alter the inferred gas kinematics because the EELRs are generally isolated from the continuum emission.

Three-color composite images including the emission line maps and a continuum band image are shown in Figure 1 to visualize the resulting flux distributions and to study the ionized gas morphology.

2.2. *Star formation histories*

Two of the host galaxies (RXJ1301 and eRO-QPE1) are spectroscopically classified as PSB (Lick index $H\delta_A > 4$ Å and EW($H\alpha$) <3 Å) or quiescent Balmer strong (QBS, $H\delta_A > 1.31$ Å) galaxies (Wevers et al. 2022). In addition, the MUSE data reveal that GSN069 and eRO-QPE2 show clear signs of ongoing star formation: GSN069 has a bright circumnuclear star-forming ring, and both GSN069 and eRO-QPE2 show several star forming knots tracing spiral arms (Figure 1). eRO-QPE3 is in the star-forming region of the BPT and WHAN diagrams, although the current star formation rate is likely low (Fig. A2).

We constrain the star formation history (SFH) by assuming that each galaxy experienced a recent burst of star formation. We constrain the post-starburst age (age since 90% of the burst stars formed) and mass of new stars that formed by modeling the integrated nuclear spectra with Bagpipes (Carnall et al. 2018, 2019). We assume a SFH consisting of an old delayed exponential and a young burst exponential, using a similar method as French et al. (2023). We allow the masses and ages of both components to vary, as well as the duration of the young burst component, with logarithmic priors. We assume a Kroupa (2001) initial mass function and a Calzetti dust law, allowing the attenuation to vary. Following Carnall et al. (2019), we include three terms in a Gaussian process noise model.

We find that when allowing for both a young and an old burst, all galaxies prefer the inclusion of a recent burst of star formation within the last 0.2-1.3 Gyr. For RXJ1301 and eRO-QPE2, our modeling prefers a sizeable recent burst (Table 1). This burst has been

quenched for RXJ1301 (hence its PSB classification), while the burst is still ongoing for eRO-QPE2 (hence its SF/AGN classification, see §3). eRO-QPE1 had a weaker burst about a Gyr ago and has remained quenched, leading to its QBS classification[1]. The burst in eRO-QPE3 is smaller still ($\sim 1-2\%$ of stars formed). Finally, the SFH of GSN069 resembles that of eRO-QPE2, including a smaller burst fraction (5% of stars formed) where the SF has not yet been fully quenched.

3. RESULTS

Upon inspection of the emission line maps (Fig. 1, top row), 3/5 sources show very extended emission line regions (EELRs) that have line ratios consistent with being powered by SF or a non-stellar continuum (Fig. 1, bottom two rows). We note that the sensitivity of our observations is not uniform across the sample, and the non-detections in two sources may be in part due to a sensitivity bias related to a higher redshift for eRO-QPE1 ($z = 0.0505$, the highest redshift in the sample), and/or a fainter and more compact host galaxy (eRO-QPE1 and eRO-QPE3).

3.1. *Extended emission line region morphology*

In Figure 1 we show continuum images of the galaxies overlaid with emission line contours of $H\alpha$ or N II (the latter is brighter in the case of GSN069 and RXJ1301). GSN069, eRO-QPE2 and RXJ1301 show EELRs on spatial scales extending up to 10 kpc from the galaxy nucleus. eRO-QPE1 and eRO-QPE3 do not show any extended ionized emission and a compact continuum morphology (Figure A1). In the case of GSN069 there are patchy clumps of gas bright only in N II which appear completely isolated to the south and south-east. There is no clear visual connection to the stellar light distribution. These EELRs do not appear to have a preferred directionality compared to the continuum morphology of their host galaxy, as might be expected if they are AGN-driven outflows or the result of stellar feedback following a strong starburst. These morphologies are instead often (but not exclusively) seen in post-merger galaxies where gas can be deposited at large radii as a result of post-merger splashback (Johnston et al. 2008; Schweizer et al. 2013; Weaver et al. 2018). However, there are other mechanisms that can result in extended gas distributions. These include galactic scale outflows powered by previous AGN activity and the accretion/infall of gas from the intergalactic medium (e.g. Hafen et al. 2019).

---

[1] We assume a specific SFH with a young and an old burst, but note that we do not explore other SFH scenarios which may also lead to a QBS classification without requiring a starburst.
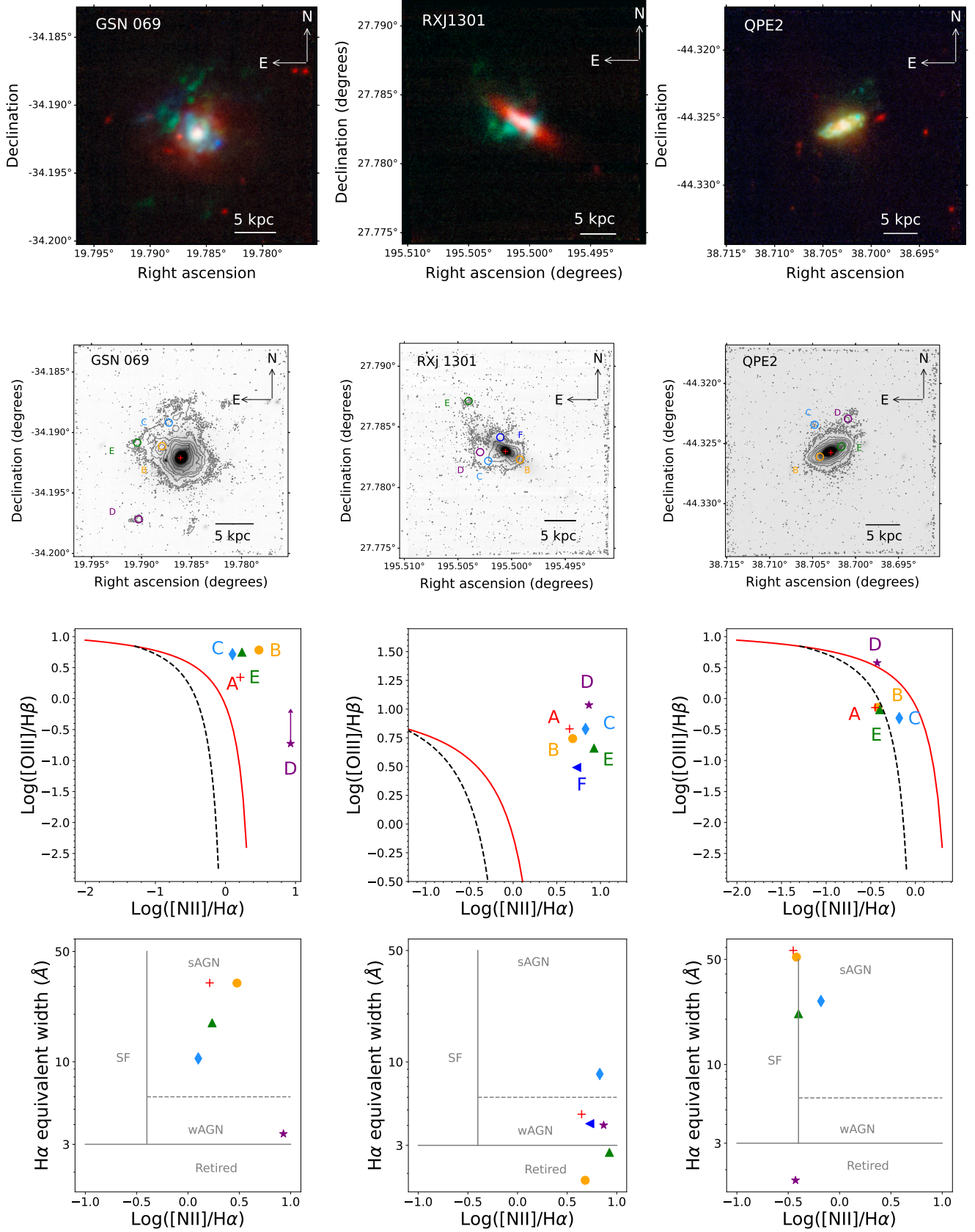
Figure 1. Images of the host galaxies. Top: RGB color composites. The continuum is shown in red, while green hues denote Hα (QPE2) or N II (RXJ1301 and GSN069). O III is shown in blue. Second row: grayscale continuum images overlaid with a contour map of the emission line. The red cross indicates the continuum nucleus position. Kilo-parsec scale extended emission line regions of ionized gas are discernable in 3/5 QPE hosts. This ionized gas is decoupled from the continuum emission. Third row: BPT diagram of the line ratios using the regions indicated in the panel above, after correcting for the stellar continuum component. Bottom row: WHAN diagram of the same regions.

3.2. *Kinematics*

Spatially resolved kinematics of the stellar and gas components are presented in Figure 2. The stellar velocity component is well-behaved and displays rotation-dominated profiles in every galaxy (shown in Figure A3 in the Appendix). The central stellar velocity dispersions we measure using aperture spectra are consistent with literature values, except for RXJ1301 and eRO-QPE3. For the former we find a value of 68 ± 5 km s^{-1}, compared to 90 ± 2 km s^{-1} measured using SDSS data (Wevers et al. 2022). This is corroborated by the spatially resolved map, which has peak values around 70 km s^{-1}. For the latter source, Arcodia et al. (2024) reported a velocity dispersion of 83 km s^{-1}, while we find $\sigma_{\rm star} = 38 \pm 5$ km s^{-1}. Using the M$_{\rm BH}$–σ relation of Gültekin et al. (2009) results in a black hole mass of M$_{\rm BH} = 5.1 \pm 0.55$ M$_\odot$ for eRO-QPE3.

The ionized gas kinematics display more disturbed patterns. In GSN069 and eRO-QPE2, the ionized gas does appear to roughly co-rotate with the stellar motions globally, although there is a velocity gradient between the gas and stars in both systems. For RXJ1301, the EELR appears to consist of a single kinematic component with a consistent velocity shift of $+50$ km s^{-1} (see Fig. 2, middle panel), completely decoupled from the rotation of the stellar motion. This is very similar to the EELR seen in the TDE host galaxy Mrk 950, presented in a companion paper (Wevers et al. submitted).

More generally, the majority of the ionized gas in these galaxies appears to have very low turbulence, with velocity dispersions that are typically <75 km $^{-1}$. We highlight that the gas in eRO-QPE2 has extremely low line widths <30 km s^{-1} throughout the galaxy and EELR. In GSN069, there are (disconnected) regions at the edge of the EELR with velocity dispersions up to 150 km s^{-1} (compared to $\sim$75 km s^{-1} in the nucleus) at distances of 7–10 kpc from the centre of the galaxy, although the bulk of the gas has $\sigma_{\rm gas} < 75$ km s^{-1}.

3.3. *Diagnostic diagrams*

We use the emission line ratios of these galaxies in diagnostic diagrams to understand the dominant ionization mechanism. The EELR pseudo-aperture spectra are located within the AGN region of the BPT and WHAN diagrams, shown in the bottom two rows of Figure 1. Our results for the galactic nuclei are consistent with the conclusion by Wevers et al. (2022) that the photo-ionization mechanism in the QPE host galaxies is likely non-stellar in nature, except for eRO-QPE3 whose ionizing continuum appears to be SF-dominated. We show the aperture spectra of various regions in Figures A4, A5 and A6 in the Appendix.

3.4. *Constraints on the ionizing luminosity*

The large extent of the EELRs can be used to probe the recent accretion history of the SMBHs in these galaxies. We follow Keel et al. (2017) and French et al. (2023) to estimate the required ionizing luminosity to power the observed EELR line fluxes. In the assumption of photo-ionization equilibrium (recombination balance), such an estimate can be made for each spaxel by taking into account the diminishing covering factor (f) with distance (the further away a spaxel is from the nucleus, the higher the required ionizing luminosity for a fixed observed line flux). More quantitatively, we follow French et al. (2023) by using the Hα and Hβ emission line luminosities L_H[2] to compute two independent estimates of L$_{\rm ion,min}$ in each spaxel (see Fig. 3.4) as follows:

$$L_{\rm ion,min} = \frac{n_r L_H E_{\rm ion}}{E_H} \frac{1}{f} \qquad (1)$$

Here, f is the covering fraction in units of spaxels,

$$f = \frac{(2 \arctan(0.5/r))^2}{4\pi} \qquad (2)$$

n_r is the number of ionizing photons per recombination, $E_{\rm ion}$ is the ionizing energy between 13.6 and 54.6 eV (we assume that higher energy photons will be primarily absorbed by Helium). E_H is the energy per Hα or Hβ photon.

Following Keel et al. (2012) we further use the Infrared Astronomical Satellite (IRAS) all-sky survey data (derived from the $60\mu m$ and $100\mu m$ measurements) to estimate the present-day AGN luminosity or derive upper limits. A correction for present-day star formation is applied based on the distance from the SF main sequence in the BPT diagram (Wild et al. 2010). These estimates are conservative given the potential for additional extinction not probed by the Balmer decrement (see e.g. Baron et al. 2022). The results can be found in Table 1. We highlight that for every QPE host with an EELR detection, we infer a present-day nuclear luminosity (L$_{\rm nuc,IR}$) that is below the luminosity required to power the most distant regions of the EELRs. In other words, if an AGN was previously present in these systems it has recently (in the last 1–3×10^4 yrs) faded in luminosity by a factor of at least 2–5. This is consistent with the episodic nature of AGN activity, which has typical duty cycles of $\sim 10^5$ years with rapid transitions on $\sim 10^4$ year timescales (Keel et al. 2017; Schawinski et al. 2015).

---

[2] Due to the relatively low SNR of spectra in individual spaxels, we do not incorporate an extinction component to estimate these line fluxes.
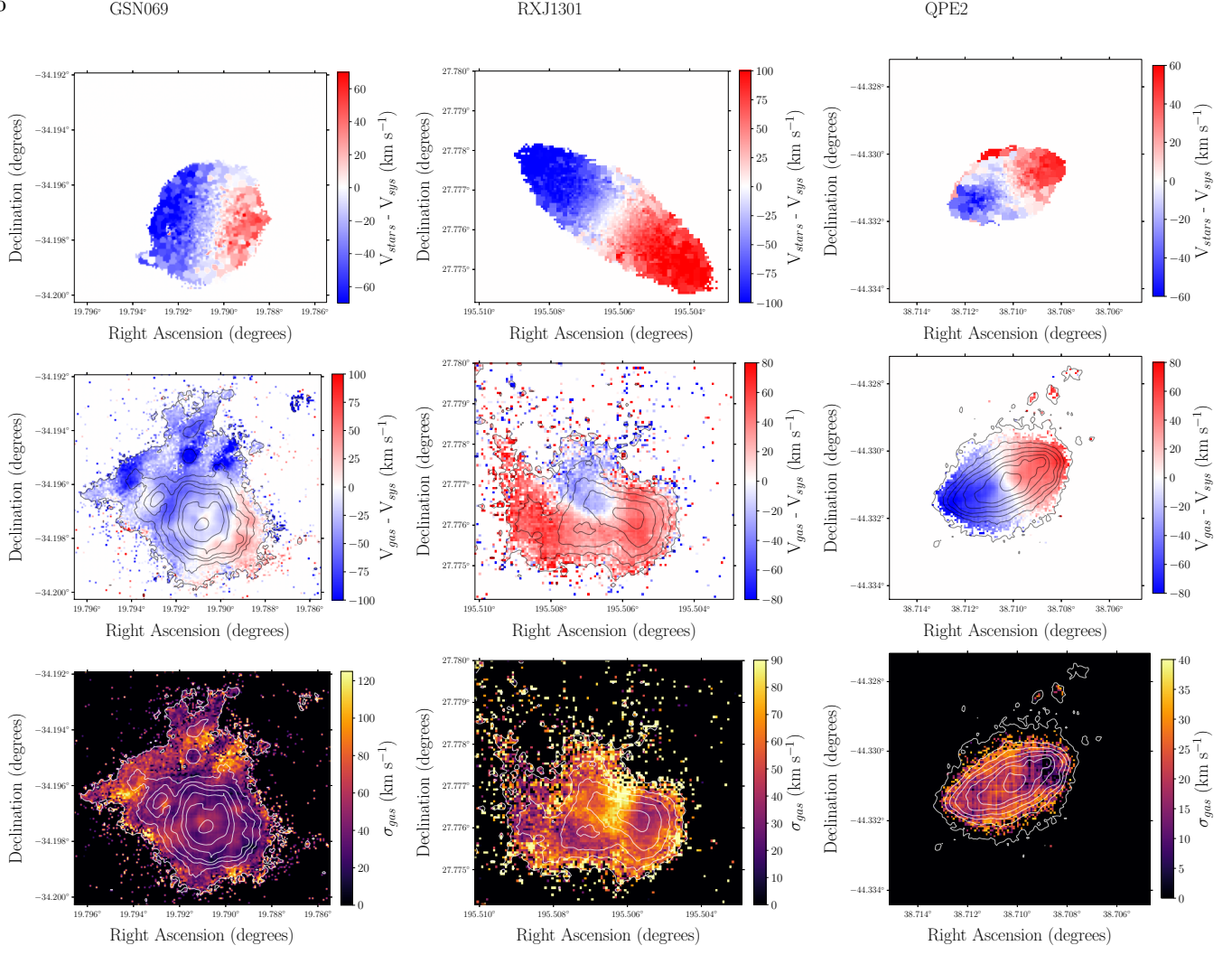
Figure 2. Spatially resolved kinematics. Stellar velocity (top), gas velocity (middle) and gas velocity dispersion (bottom) maps. The contours indicate the EELR to guide the eye. The left column shows GSN069, while the middle column shows RXJ1301 and eRO-QPE2 is shown in the right-most column. The sky area is identical for every source across the panels to highlight the differences in EELR kinematics compared to the stellar continuum.

Table 1. Overview of the QPE and EELR properties of the host galaxies. Class indicates the spectroscopic classification based on the Hδ_A absorption and Hα EW: post-starburst (PSB), quiescent Balmer strong (QBS) or neither (N). Burst age and fraction refer to the time since the most recent starburst and the percentage of stars formed in said starburst (see text), where numbers in brackets denote uncertainty on the last digit. Ion. cont. indicates the classification of the ionizing continuum, based on the BPT and WHAN diagnostic diagrams. R_{max} refers to the largest (projected) extent of the EELR relative to the nucleus. $L_{QPE,quiesc}$ is the bolometric luminosity during QPE quiescence, taken from the literature. $L_{ion,min}$ is the minimum nuclear ionizing luminosity required to power the EELR. L_{IR} is the luminosity inferred from IRAS FIR detections or upper limits.

Source	Class	Burst age $\log_{10}(\mathrm{yr})$	Burst frac.	EELR	Ion. cont. (EELR)	R_{max} (lightyr)	$L_{QPE,quiesc}$ (erg s^{-1})	$L_{ion,min}$ (erg s^{-1})	$L_{nuc,IR}$ (erg s^{-1})
GSN069	N	Ongoing	0.045(2)	Y	Non-stellar	30 000	$3\pm2\times10^{42}$	$>6\times10^{42}$	$<3\times10^{42}$
RXJ1301	PSB	8.68(1)	0.12(1)	Y	Non-stellar	9 000	$2.5\pm0.5\times10^{42}$	$>2.5\times10^{42}$	$<1.5\times10^{42}$
eRO-QPE1	QBS	9.11(4)	0.066(2)	N	—	—	$5.1^{+1.6}_{-1.5}\times10^{40}$	—	—
eRO-QPE2	N	Ongoing	0.14(2)	Y	Composite	15 000	$3^{+4}_{-2}\times10^{43}$	$>2.5\times10^{42}$	4×10^{41}
eRO-QPE3	N	8.6(2)	0.014(1)	N	—	—	$<4\times10^{40}$	—	—
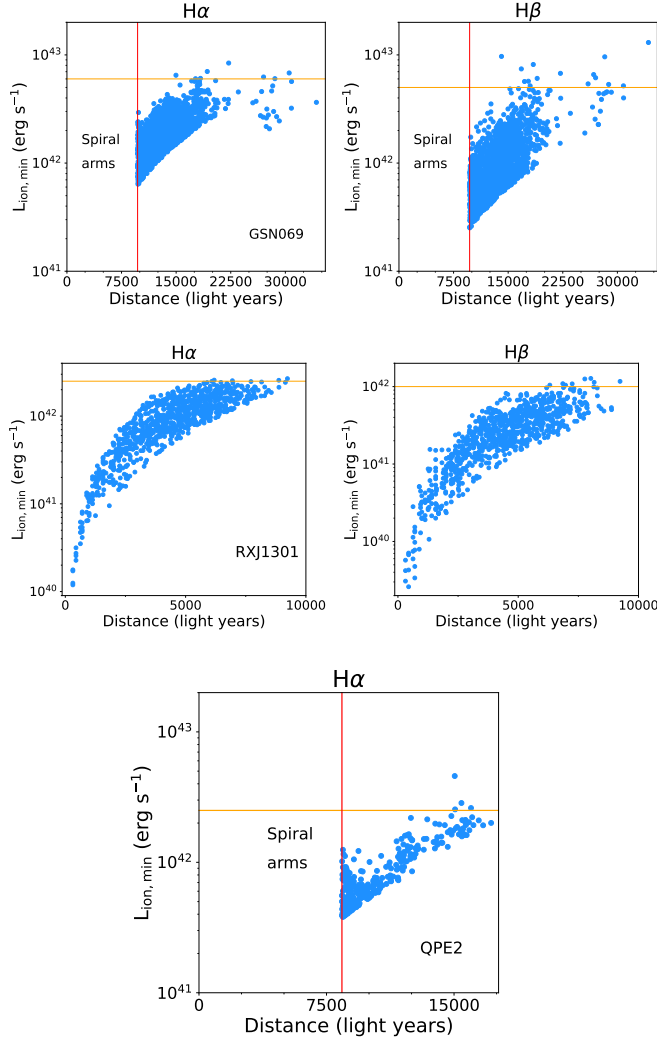
Figure 3. Constraints on the ionizing luminosity. Every data point represents the minimum required ionizing luminosity to explain the EELR (indicated by the orange horizontal line), assuming recombination balance, for an individual spaxel. The inner regions of GSN069 and eRO-QPE2 are actively star-forming, so are excluded for clarity (marked by the red vertical lines).

4. DISCUSSION

Our analysis shows that 4/5 QPE host galaxies have one or more peculiar properties, including the presence of a quenched starburst (a post-starburst phase, RXJ1301), a quiescent Balmer strong spectrum (which may indicate a weaker recent starburst, eRO-QPE1), the presence of extended ionized gas emission (Fig. 2, RXJ1301, GSN 069 and eRO-QPE2) that is decoupled from the stellar continuum, and/or the presence of a recently faded nuclear engine in three systems (Table 1, RXJ1301, GSN 069 and eRO-QPE2). The latter occurs in ∼1/3 of EELR hosting galaxies (Keel et al. 2012), so

the unity fraction observed here may be another peculiar characteristic of QPE hosts but requires confirmation with larger samples. No tidal tails or other visual disturbances are obvious in the stellar continuum light. Such features are typically seen in other studies of Voorwerp / faded AGNs with EELRs (e.g. Keel et al. 2015), and they provide a robust association for a post-merger origin of the EELR gas. We note that at present we do not have similarly compelling evidence for a post-merger origin because our observations are relatively shallow and have poor spatial resolution. Further studies of larger samples are needed to confirm the tentative connection between the QPE host properties and post-merger faded AGNs with EELRs.

We find a fractional incidence of EELRs in QPE host galaxies of $f_{EELR} = 0.6^{+0.4}_{-0.33}$ (where the uncertainties are two-sided Poisson confidence intervals, Gehrels 1986).

We compare this to literature values with the caveat that the galaxy samples are not matched in properties (e.g., redshift, stellar mass, depth of observation) because only a few statistical studies exist. The QPE host EELR incidence is a factor of ∼10 higher than the fraction of EELRs found in the general galaxy population, $f_{EELR} \sim 0.085$, although a large number of these are SF- or AGN-driven outflows (López-Cobá et al. 2020) which is not the case for the EELRs discovered in this work. The incidence of EELRs in QPE hosts is a factor of ∼30 higher than in AGN host galaxies ($f_{EELR} = 0.023 \pm 0.013$, Keel et al. 2024).

Compared specifically to PSB (E+A) galaxies, French et al. (2023) found the EELR incidence to be $f_{EELR} = 0.065^{+0.035}_{-0.025}$, and hence we infer an overrepresentation by a factor of ∼10× even compared to this rare type of post-merger galaxy comprising less than 0.2 per cent of the local galaxy population (Zabludoff et al. 1996). The EELR fraction of QPE hosts is similar to that seen in post-merger galaxies identified through the presence of tidal tails and interaction with companion galaxies in continuum light (Keel et al. 2024). The lack of similar tidal features may indicate that the QPE hosts are not post-merger (Section 3.1), or that the merger occurred ∼1 Gyr ago, short enough that we still see the post-merger signatures such as extended reservoirs of gas but long enough that most obvious merger features (e.g. dust lanes, tidal tails) have already faded (Pawlik et al. 2016).

With the caveat of small sample statistics, we note that the overrepresentation of EELRs in QPE hosts is somewhat higher than that found in TDE host galaxies ($f_{EELR} = 0.19^{+0.14}_{-0.11}$ for the entire sample with MUSE observations, Wevers et al. submitted) but consistent with the PSB-TDE-EELR host galaxies ($f_{EELR} = 0.6^{+0.4}_{-0.33}$,

Wevers et al. submitted)[3]. The implication is that there may be a connection between these two classes of nuclear transients, which we explore further below.

4.1. The QPE–TDE host galaxy connection

In a companion paper (Wevers et al. submitted) we analyzed MUSE observations of 16 TDE host galaxies. Combined with previously known EELRs in TDE hosts, we inferred an elevated EELR incidence compared to post-starburst galaxies as well as the general galaxy population. The overabundance of EELRs among TDE hosts is a factor of $10\times$ compared to post-starburst galaxies, which is similar to the overrepresentation reported for QPE hosts in this work.

In addition, the QPE host galaxy EELRs show peculiar kinematics that are strikingly similar to those of the EELR-hosting TDE host galaxies. The combination of non-stellar photo-ionization, a recently faded AGN, low velocities and low velocity dispersions is rare among the general galaxy population (< 1 per cent), although this is based on HST narrow-band imaging rather than IFU observations (Keel et al. 2012, 2024). These properties are inconsistent with AGN- or shock-driven kinematics and associated ionization mechanism.

A tentative connection between the QPE phenomenon and TDEs has been proposed based on the observational properties of QPEs, including long-term declines in the continuum X-ray lightcurves (Miniutti et al. 2019, 2023; Arcodia et al. 2024), the presence of a single QPE-like flare in the decay of some TDE candidates (Chakraborty et al. 2021; Quintin et al. 2023) and the PSB/QBS preference of the host galaxies (Wevers et al. 2022). Moreover, several theoretical models invoke partial TDEs as a mechanism to render a (pre-existing) closely bound stellar remnant visible as it interacts with the newly formed, compact accretion disk. Such models strongly disfavor the presence of a large AGN accretion disk because ablation of the star would severely shorten the lifetime of the QPE source (Linial & Metzger 2024).

The tentative connection between TDEs and QPEs can also be investigated using sample properties as is done here. Our results provide the strongest, albeit indirect, indication to date that QPE and TDE rates are enhanced in gas-rich environments with faded AGNs, and possibly in post-merger systems[4]. The implication could be that they share a common formation path, although the implications of this host galaxy connection

depend on the theoretical scenario invoked to explain QPEs.

4.2. The QPE–EELR connection

Our analysis shows that the QPE quiescent luminosity can in principle reach the threshold required to power the EELR energy budget (i.e. $L_{QPE,quiesc} \gtrsim L_{ion,min}$) in RXJ1301, eRO-QPE2, but not in GSN069[5] (see Table 1). The quiescent luminosity of the 2 host galaxies without EELRs are the lowest among the sample. More generally, with the low duty cycle of QPEs ($\sim 25\%$, Guolo et al. 2024) and their unknown but likely limited lifetime[6] it appears improbable that the eruptions alone can power the EELRs. We note, however, that some scenarios require a (partial) TDE to occur before QPEs can be detected. As TDEs typically have a larger energy budget available, it is in principle possible to power the EELRs through a (time-limited) increase in the TDE rate by a factor of ~ 10 compared to the average TDE rate in PSB galaxies (Wevers et al. submitted). Depending on the relative rate of TDEs and QPEs, it may therefore also be possible that the EELRs are powered (in part) by episodic accretion in the form of an elevated TDE rate, rather than a classical AGN phase.

4.3. Implications for the nature of QPEs
4.3.1. Partial TDE scenario

The fact that both QPEs and TDEs prefer host galaxies with similar, peculiar properties can point to an intrinsic connection between these classes of events. In this case, the most obvious link may be through the disturbed state of the galactic nuclei following a (minor) galaxy merger. This would perturb the orbits of stars in the nucleus and lead to an increased rate of star-SMBH encounters of all kinds, including full tidal disruptions, partial TDEs and even direct captures. QPEs have been linked to partial TDEs, where the Hills mechanism can disrupt a binary star system to capture one of the components on a tight eccentric orbit, leading to the repeated partial stripping at each pericentre passage or alternatively direct mass transfer (e.g. King 2022; Krolik & Linial 2022; Linial & Sari 2023; Lu & Quataert 2023; Metzger et al. 2022; Zhao et al. 2022). In this scenario, repeating nuclear transients on all timescales would likely share a common formation channel and therefore host galaxy preference, even though they may

---

[3] We emphasize that the sensitivity of the IFU observations is not uniform across the QPE and TDE samples.

[4] For the QPEs, this statement relies on a single PSB galaxy, RXJ1301.

[5] Note that the long-term luminosity behavior of this source is highly variable and was significantly higher in the past (with $L_{QPE,quiesc} > L_{ion,min}$).

[6] In the star-disk interaction models, it is <1000 yrs (Linial & Metzger 2024).

not share the same observational properties (e.g. Guolo et al. 2024). This idea can be tested through a host galaxy study of a more inclusive set of repeating nuclear transients, including QPEs and partial TDEs recurring on timescales of 10s/1000s of days (e.g. Payne et al. 2021; Wevers et al. 2023; Liu et al. 2023; Guolo et al. 2024).

4.3.2. *Star-disk / BH-disk interaction scenario*

In addition to the partial TDE scenario, there exist related but distinct theoretical models to explain QPEs. For example, the rate and lifetime of EMRIs is sufficiently high that a pre-existing bound stellar-mass companion is expected to be present in numerous galactic nuclei (Linial & Metzger 2024). Rendering such systems visible is possible if a TDE provides a compact accretion disk with which the bound remnant periodically interacts, leading to the QPE phenomenon (Linial & Metzger 2023). In this scenario there is a natural commonality between the host galaxies of QPEs and TDEs, as the latter are required to observe the former. One distinction with the pTDE models is that the typical lifetime of the QPE (set by the ablation timescale of the star while interacting with the disk) is at most 1000 years, and the implication is that the QPEs themselves cannot be invoked as the powering source for the EELR (because their extent is $>10^4$ yrs). A preference for post-starburst galaxies was predicted in this scenario, as such systems are more likely to host EMRIs in the first place (Metzger et al. 2022).

4.3.3. *Accretion disk instability scenario*

Alternatively, QPEs have also been suggested to be caused by instabilities in large AGN-like disks (e.g. Sniegowska et al. 2020; Raj & Nixon 2021; Pan et al. 2023). On one hand, it seems less likely that the connection between QPEs and TDEs is intrinsic in this case. The TDEs found in EELR-hosting galaxies are unremarkable in the context of the known TDE sample, while it has been predicted that AGN disks may significantly alter the observed properties (Chan et al. 2019). On the other hand, it has been proposed that the presence of an AGN disk may significantly increase the TDE rate (e.g. Kennedy et al. 2016; Wang et al. 2024; Kaur & Stone 2024). All three QPE nuclei with EELRs have faded in the recent past, which has been suggested to result in a higher TDE rate due to star-disk interactions and the presence of stars formed in the outer regions of the accretion disk (Wang et al. 2024), or alternatively through an enhanced loss cone filling rate through collisionless processes in gas-rich nuclei (Kaur & Stone 2024).

We highlight that based on X-ray spectral modeling, the neutral (and ionizing) absorbing columns are very low: $N_H \simeq 4 \times 10^{21}$ cm^{-2} [E(B-V)~0.6, Güver & Özel 2009] for eRO-QPE2, and $N_H < 5 \times 10^{20}$ cm^{-2} [E(B-V)<0.07] for all others, i.e., QPE nuclei are completely unobscured. Nevertheless, no broad emission lines are detectable in deep long-slit data (Wevers et al. 2022) nor in our MUSE observations. For the source GSN 069, the present-day continuum (quiescent) bolometric luminosity is of order few $\times 10^{43}$ erg s^{-1}, and hence this lack of broad emission lines (BELs) is unlikely to be the consequence of a too low nuclear luminosity. Instead it may be related to the presence of a disk that is too compact to support a typical broad line region (BLR), which is compatible with the accretion disks that form in the aftermath of a TDE (for which several lines of evidence exist in GSN 069, Sheng et al. 2021; Miniutti et al. 2023; Patra et al. 2024). Pan et al. (2023) argue that while QPEs do require some fine-tuning (e.g., a very small unstable region, peculiar magnetic field, etc.), it is possible, in principle, that these conditions are only met in compact TDE disks but inefficient in much larger AGN disks.

The current weak state of the nuclei (compared to a more luminous state in the past, required by the EELR energy budget) may be the result of a selection bias against QPEs in higher luminosity AGN. It may be more difficult to detect the QPEs as an additional component on top of the AGN continuum emission (Miniutti et al. 2023) which may be highly variable, especially so for low black hole masses (e.g. Ponti et al. 2012). Similarly, the TDE detection rate may be biased against AGN host galaxies because of spectroscopic selection biases. In this scenario the selection biases in both TDEs and QPEs would need to *conspire* to create the observed similarities and preferences in an extremely rare type of host galaxy. This scenario is somewhat contrived, but ruling it out completely will only be possible with larger samples of QPE and TDE host galaxies.

4.4. *Localization of low frequency gravitational wave sources*

Maximizing the scientific value of GW sources will be facilitated by complementary EM information such as the host redshift, galaxy/black hole mass, and stellar population properties. Due to the poor sky localization of LISA GW detections (typically of order a degree or larger), the number of galaxies within the error volume will be very large (Lops et al. 2023). Simulations show that it is very challenging to uniquely identify the host galaxies of GW sources. This is because the preferred host galaxies are dwarfs with merger signatures, but a

large fraction of the dwarf galaxy population will exhibit very similar signatures (Izquierdo-Villalba et al. 2023).

However, we have found that QPE sources (as well as TDEs, Wevers et al. submitted) are strongly overrepresented in galaxies hosting recently faded AGNs and large EELRs with peculiar kinematical properties. Galaxies with similar properties are very rare among the general galaxy population, and hence if the association of QPEs with stellar-mass EMRIs can be confirmed, these peculiar properties can be used to improve the fidelity of EMRI host galaxy localization, which will help to maximize the scientific return of GW astronomy.

Because the X-ray eruptions have a low duty cycle (Guolo et al. 2024) and potentially short lifetimes (<1000 years, e.g. Linial & Metzger 2023), it is likely that QPEs will be detected in only a small subset of GW detections (see also e.g. Franchini et al. 2023, who show that only ∼2% of BH EMRIs would produce detectable QPEs). Making associations through their host galaxies can therefore be a valuable complementary method to find EM counterparts.

5. CONCLUSIONS

We report on the analysis of MUSE integral field spectroscopy of the host galaxies of five quasi-periodic X-ray eruption (QPE) sources. The sensitivity, large field of view and small spaxel size of MUSE provide an unprecedented, spatially resolved view of the QPE host galaxies. We measure the stellar and emission line kinematics, fluxes and flux ratios to characterize their properties.

We find that three out of five galaxies have extended emission line regions that have low velocities which are decoupled from the stellar motions. The emission line ratios require a hard non-stellar continuum as the source of the ionizing photons, but the very narrow line velocity dispersions and low velocities are inconsistent with these EELRs being driven by a currently active nucleus. Furthermore, no broad emission lines are observed, which together with the lack of significant obscuration could suggest that no classical BLR region is present[7].

The present-day nuclear luminosity estimated from FIR observations is insufficient to satisfy the EELR energy budget, implying that the putative AGNs in these nuclei have decreased their luminosity output significantly in the recent past (9 000–30 000 yrs, limited by the extent of the EELR). This could suggest a connection between either the intrinsic rate or the detection rate of QPEs and the specific phase in the AGN duty cy-

cle. The overrepresentation of EELRs in the QPE host galaxies is roughly an order of magnitude compared to post-starburst galaxies, and in combination with the peculiar kinematics, potentially even higher compared to the general galaxy population.

Several properties of the QPE host galaxies are similar to those of TDE host galaxies. Both classes have a preference for QBS/PSB galaxies (French et al. 2016; Wevers et al. 2022), a strong overrepresentation of EELRs with recently faded nuclei, and peculiar ionized gas kinematic properties (studied in detail for TDE hosts in a companion paper, Wevers et al. submitted). The rarity of the preferred type of host galaxies is highly unlikely to be due to chance, and is robust against associations based on the unique properties of individual QPE sources. This strongly suggests a connection between these two classes of events, consistent with theoretical arguments and hinted at in the observational properties of individual sources (Miniutti et al. 2023; Arcodia et al. 2024).

The proposed link between QPEs and TDEs disfavors AGN accretion disk models as the origin of QPEs, as i) the AGNs are currently inactive, and ii) this would be the result of two independent selection biases (a detection bias for QPEs, and a detection and/or classification bias for TDEs). The instabilities proposed as the origin for QPEs are typically not "standard" thermal instabilities. Most require some fine-tuning (e.g. magnetic fields inducing very small unstable regions, or independently precessing rings in the case of disc tearing) that are not expected in long-lived large AGN-like discs.

More detailed studies, including deep narrow-band imaging and/or higher spatial resolution IFU observations, of both QPE and TDE host galaxies can be used to further test the similarity of the host galaxy preferences of these transients. Larger samples can be used to further characterize the properties of these host galaxies and predictions for EMRI GW sources. If these galaxies can be typed by machine learning algorithms, this may facilitate the localization of low frequency GW detections with future observatories.

---

[7] We note that our observations do not have sufficient spatial resolution to robustly rule out the presence of faint broad emission lines.

Table A1. Overview of the QPE host galaxies analyzed in this work. Spatial resolution refers to the native 0.2 arcsec pixel scale of the MUSE WFM-NOAO observations. The PSF FWHM is estimated using point sources in the continuum cube when available, or otherwise taken as the average seeing conditions (uncorrected for airmass) provided by the observatory (marked with an asterisk) as tabulated in Table A2. $\sigma_{\rm star}$ provides the central velocity dispersion, measured using an aperture with the size of the PSF FWHM.

Source	z	Spatial resolution (pc / pix)	PSF FWHM (arcsec)	PSF FWHM (pc)	E(B–V)$_{\rm gal}$ (mag)	$\sigma_{\rm star}$ km s^{-1}	Reference
GSN069	0.0182	74	1.0	370	0.0232	68±12	Saxton et al. (2011)
RXJ1301	0.0237	96	0.94*	450	0.0077	68±5	Dewangan et al. (2000)
eRO-QPE1	0.0505	199	0.95*	940	0.0212	66±4	Arcodia et al. (2021)
eRO-QPE2	0.0175	71	0.7	250	0.0153	38±6	Arcodia et al. (2021)
eRO-QPE3	0.024	97	0.7	340	0.0505	38±5	Arcodia et al. (2024)

Facilities: ESO/VLT

Software: astropy (Astropy Collaboration et al. 2013, 2018)

APPENDIX

SUPPLEMENTARY MATERIAL

REFERENCES

Arcodia, R., Merloni, A., Nandra, K., et al. 2021, Nature, 592, 704, doi: 10.1038/s41586-021-03394-6

Arcodia, R., Liu, Z., Merloni, A., et al. 2024, A&A, 684, A64, doi: 10.1051/0004-6361/202348881

Astropy Collaboration, Robitaille, T. P., Tollerud, E. J., et al. 2013, A&A, 558, A33, doi: 10.1051/0004-6361/201322068
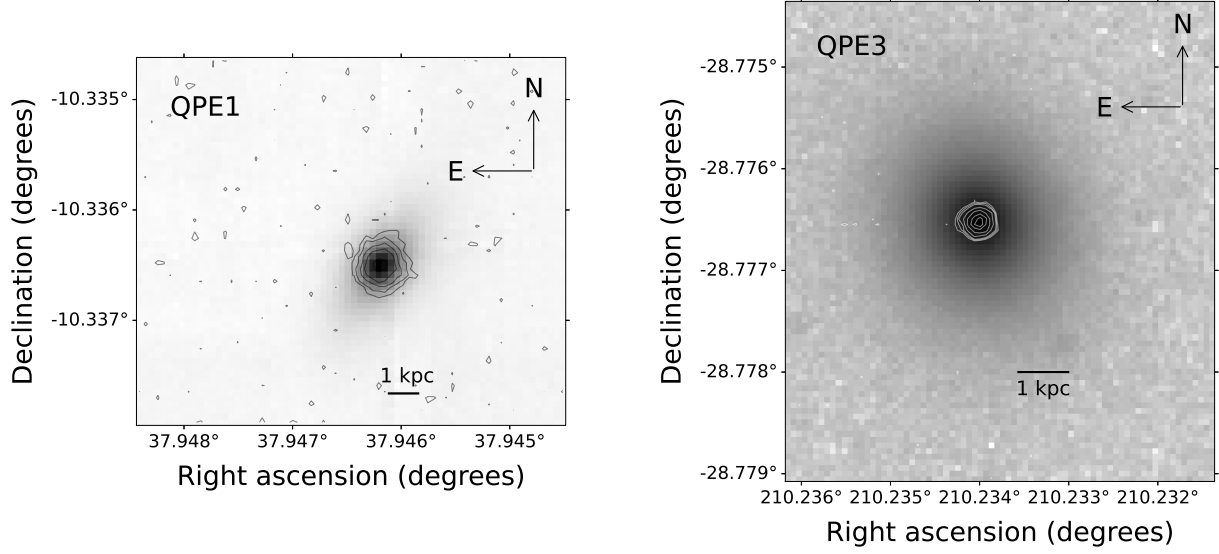
Figure A1. Continuum grayscale image and Hα contours overlaid for the source eRO-QPE1 (left) and eRO-QPE3 (right), which do not show an EELR. The faintest contours represent Hα flux levels of $35\times\ 10^{-20}$ erg cm^{-2} s^{-1} Å and $15\times\ 10^{-20}$ erg cm^{-2} s^{-1} Å for eRO-QPE1 and eRO-QPE3, respectively.
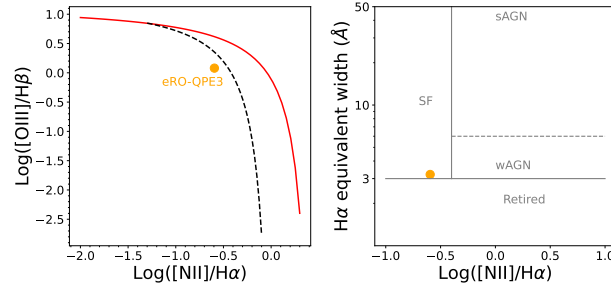
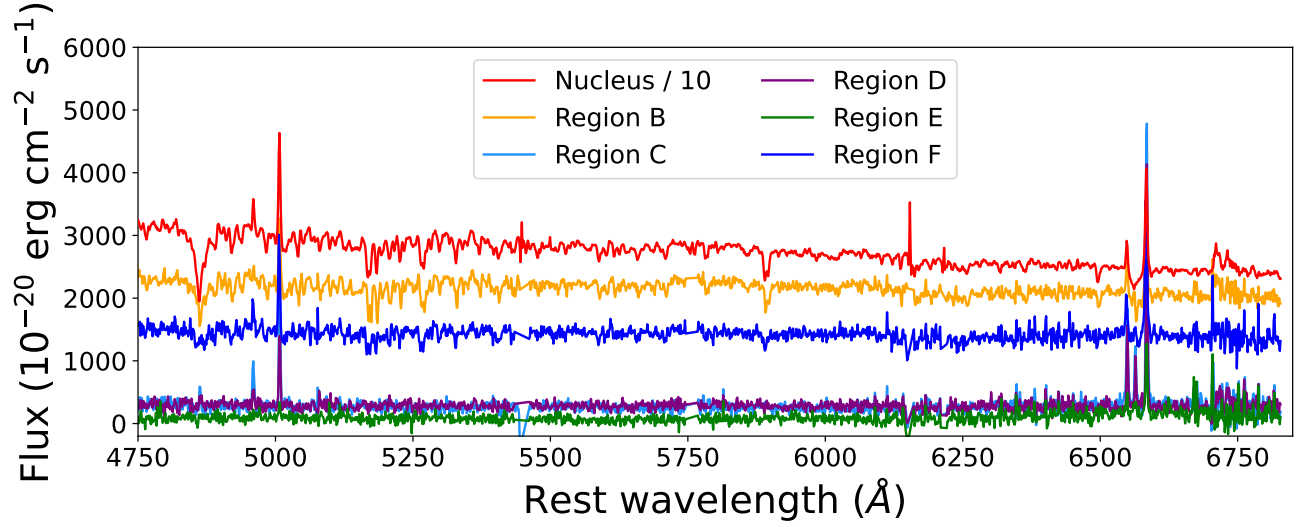**Figure A2.** BPT and WHAN diagram for the source eRO-QPE3.
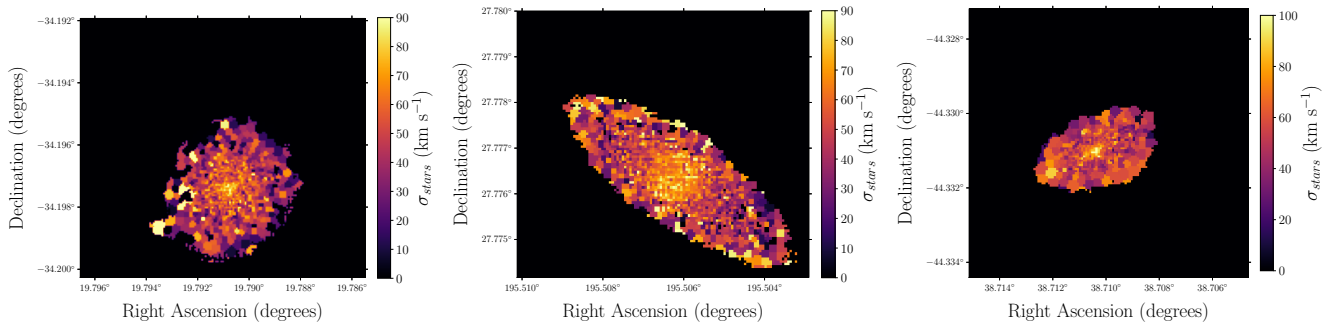
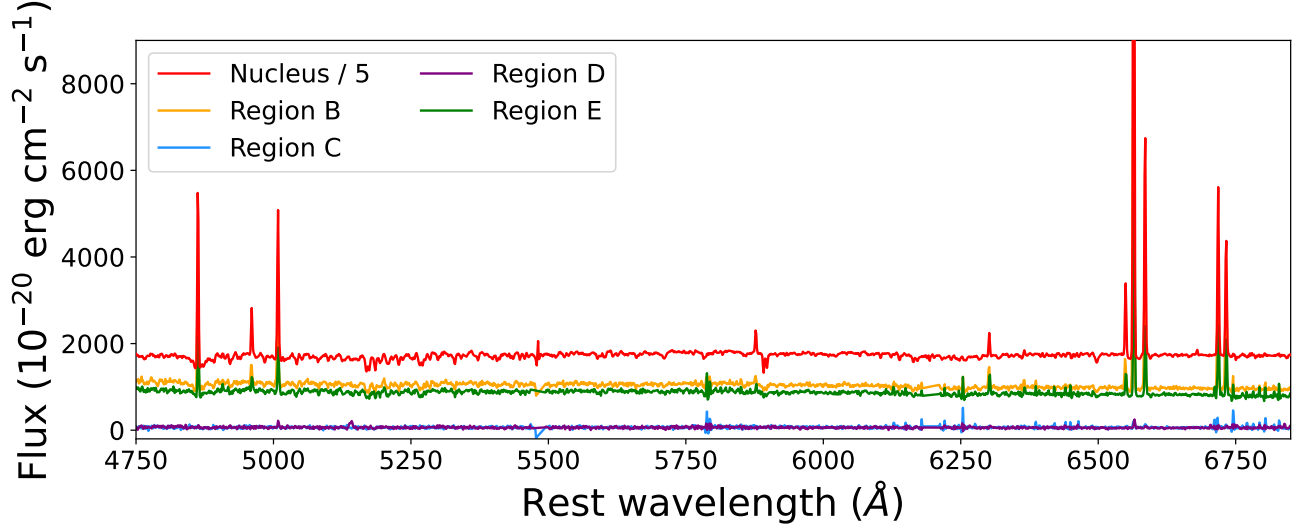**Figure A3.** Stellar velocity dispersion maps of GSN069 (left), RXJ1301 (middle) and eRO-QPE2 (right).
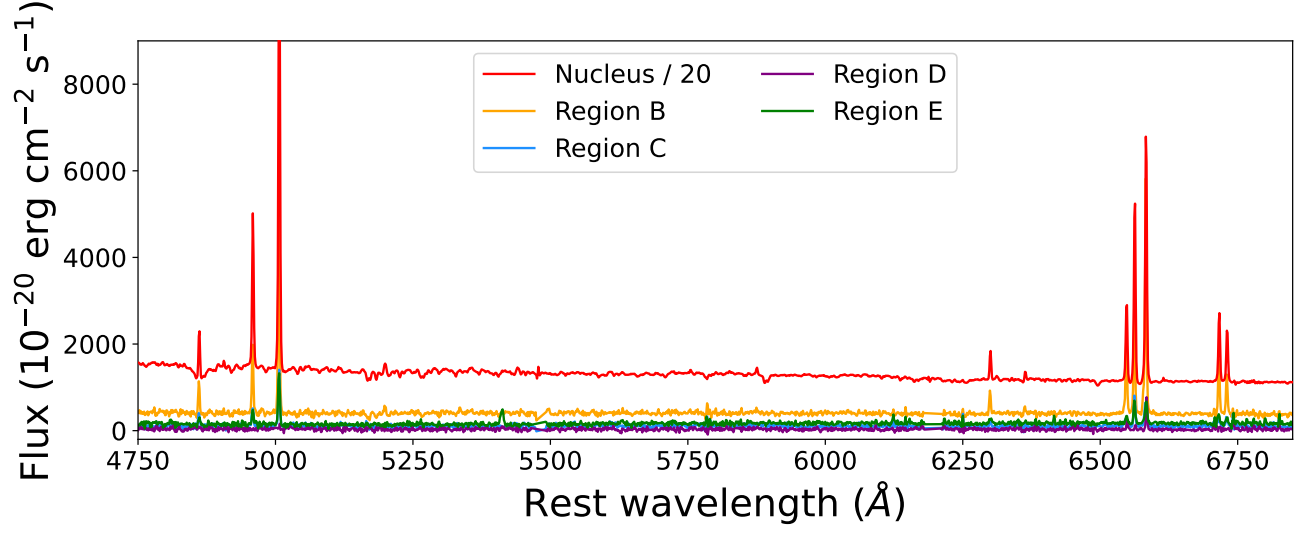
Figure A4. Aperture spectra of GSN069, for the regions indicated in Figure 1, with the same color coding.

Figure A5. Aperture spectra of RXJ1301, for the regions indicated in Figure 1, with the same color coding.

Figure A6. Aperture spectra of eRO-QPE2, for the regions indicated in Figure 1, with the same color coding.

Table A2. Observing log of the VLT/MUSE data. All data was taken in Wide Field no-AO Mode with the nominal filter.

Source	Date (MJD)	Exposure time (Seconds)	Airmass	DIMM seeing (arcsec)
GSN069	59787.237738	1497	1.64	0.53
	59787.256443	1497	1.46	0.73
RXJ1301	59787.966968	1497	1.92	1.10
	59787.985819	1497	2.11	0.78
eRO-QPE1	59834.144255	1497	2.25	1.11
	59834.162944	1497	1.86	0.75
	59834.263008	1497	1.11	1.03
	59834.281717	1497	1.07	1.04
	59834.303142	1497	1.04	0.74
	59834.321856	1497	1.03	0.87
	59834.343499	1497	1.04	1.04
	59834.362185	1497	1.06	0.98
eRO-QPE2	59787.369579	1497	1.18	0.63
	59787.388267	1497	1.13	0.51
	59814.263422	1497	1.30	2.19
	59814.282118	1497	1.23	0.97
eRO-QPE3	60416.343266	1497	1.352	4.84
	60416.361829	1498	1.498	4.84
	60432.108992	1492	1.060	0.33
	60432.127534	1493	1.029	0.44
	60435.208337	1480	1.041	1.21
	60435.226639	1480	1.078	1.16
	60438.139092	1487	1.005	0.81
	60438.157507	1488	1.003	0.64
	60439.167192	1486	1.008	0.78
	60439.185699	1486	1.025	0.85
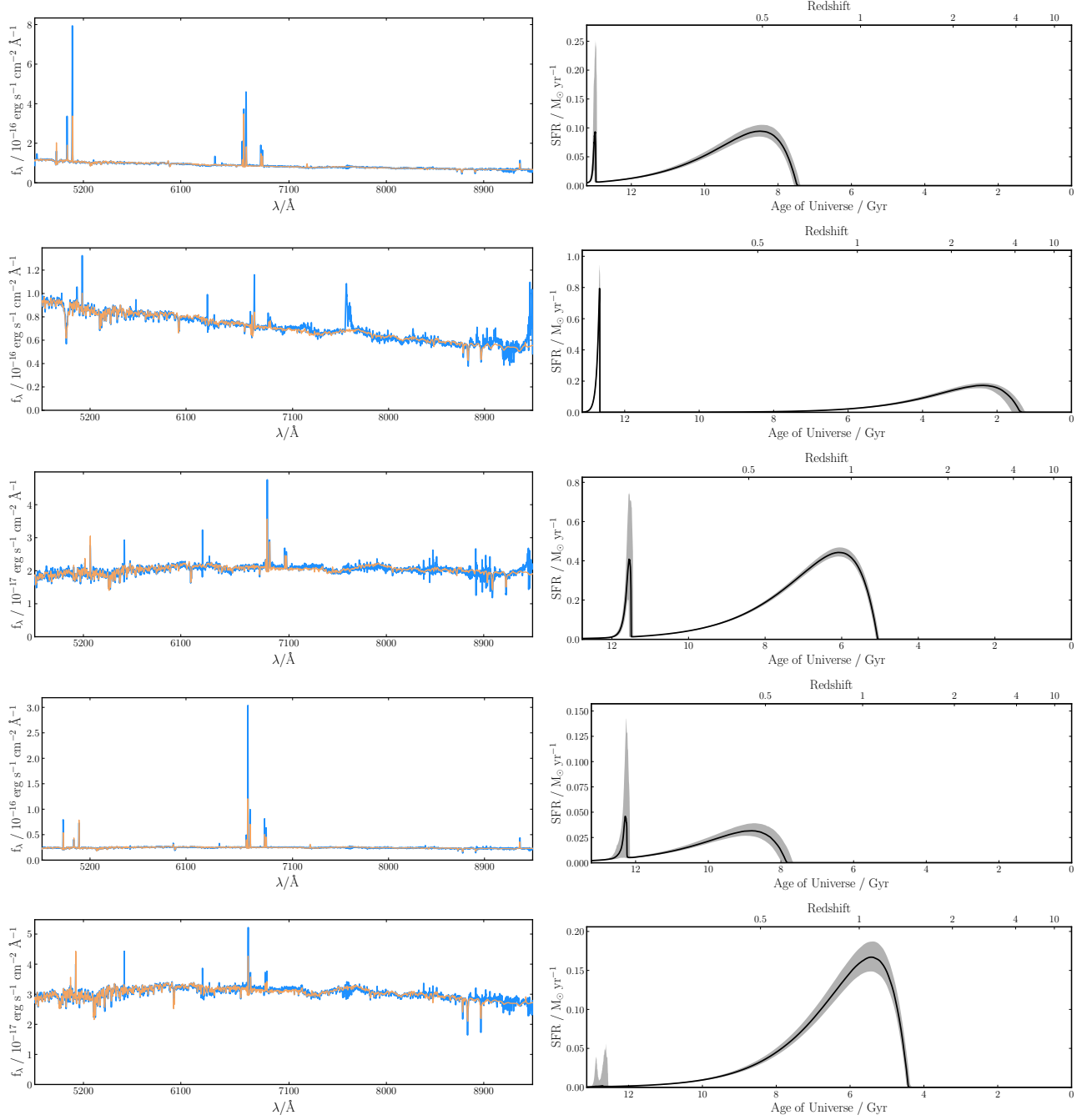
Figure A7. Bagpipes fits and inferred star formation history, assuming a double starburst as detailed in the text. From top to bottom: GSN069, RXJ1301, eRO-QPE1, eRO-QPE2, and eRO-QPE3.

Astropy Collaboration, Price-Whelan, A. M., Sipőcz, B. M., et al. 2018, AJ, 156, 123, doi: 10.3847/1538-3881/aabc4f

Bacon, R., Accardo, M., Adjali, L., et al. 2010, in Society of Photo-Optical Instrumentation Engineers (SPIE) Conference Series, Vol. 7735, Ground-based and Airborne Instrumentation for Astronomy III, ed. I. S. McLean, S. K. Ramsay, & H. Takami, 773508, doi: 10.1117/12.856027

Baron, D., Netzer, H., Lutz, D., Prochaska, J. X., & Davies, R. I. 2022, MNRAS, 509, 4457, doi: 10.1093/mnras/stab3232

Cappellari, M. 2023, MNRAS, 526, 3273, doi: 10.1093/mnras/stad2597

Carnall, A. C., McLure, R. J., Dunlop, J. S., & Davé, R. 2018, MNRAS, 480, 4379, doi: 10.1093/mnras/sty2169

Carnall, A. C., McLure, R. J., Dunlop, J. S., et al. 2019, MNRAS, 490, 417, doi: 10.1093/mnras/stz2544

Chakraborty, J., Kara, E., Masterson, M., et al. 2021, ApJL, 921, L40, doi: 10.3847/2041-8213/ac313b

Chan, C.-H., Piran, T., Krolik, J. H., & Saban, D. 2019, ApJ, 881, 113, doi: 10.3847/1538-4357/ab2b40

Dewangan, G. C., Singh, K. P., Mayya, Y. D., & Anupama, G. C. 2000, MNRAS, 318, 309, doi: 10.1046/j.1365-8711.2000.03755.x

Franchini, A., Bonetti, M., Lupi, A., et al. 2023, A&A, 675, A100, doi: 10.1051/0004-6361/202346565

French, K. D., Arcavi, I., & Zabludoff, A. 2016, ApJL, 818, L21, doi: 10.3847/2041-8205/818/1/L21

French, K. D., Earl, N., Novack, A. B., et al. 2023, ApJ, 950, 153, doi: 10.3847/1538-4357/acd249

Gehrels, N. 1986, ApJ, 303, 336, doi: 10.1086/164079

Giustini, M., Miniutti, G., & Saxton, R. D. 2020, A&A, 636, L2, doi: 10.1051/0004-6361/202037610

Graur, O., French, K. D., Zahid, H. J., et al. 2018, ApJ, 853, 39, doi: 10.3847/1538-4357/aaa3fd

Gültekin, K., Richstone, D. O., Gebhardt, K., et al. 2009, ApJ, 698, 198, doi: 10.1088/0004-637X/698/1/198

Guolo, M., Pasham, D. R., Zajaček, M., et al. 2024, Nature Astronomy, 8, 347, doi: 10.1038/s41550-023-02178-4

Güver, T., & Özel, F. 2009, MNRAS, 400, 2050, doi: 10.1111/j.1365-2966.2009.15598.x

Hafen, Z., Faucher-Giguère, C.-A., Anglés-Alcázar, D., et al. 2019, MNRAS, 488, 1248, doi: 10.1093/mnras/stz1773

Izquierdo-Villalba, D., Colpi, M., Volonteri, M., et al. 2023, A&A, 677, A123, doi: 10.1051/0004-6361/202347008

Johnston, K. V., Bullock, J. S., Sharma, S., et al. 2008, ApJ, 689, 936, doi: 10.1086/592228

Kaur, K., & Stone, N. C. 2024, arXiv e-prints, arXiv:2405.18500. https://arxiv.org/abs/2405.18500

Keel, W. C., Moiseev, A., Uklein, R., & Smirnova, A. 2024, MNRAS, 530, 1624, doi: 10.1093/mnras/stae946

Keel, W. C., Chojnowski, S. D., Bennert, V. N., et al. 2012, MNRAS, 420, 878, doi: 10.1111/j.1365-2966.2011.20101.x

Keel, W. C., Maksym, W. P., Bennert, V. N., et al. 2015, AJ, 149, 155, doi: 10.1088/0004-6256/149/5/155

Keel, W. C., Lintott, C. J., Maksym, W. P., et al. 2017, ApJ, 835, 256, doi: 10.3847/1538-4357/835/2/256

Kennedy, G. F., Meiron, Y., Shukirgaliyev, B., et al. 2016, MNRAS, 460, 240, doi: 10.1093/mnras/stw908

King, A. 2022, MNRAS, 515, 4344, doi: 10.1093/mnras/stac1641

Krolik, J. H., & Linial, I. 2022, ApJ, 941, 24, doi: 10.3847/1538-4357/ac9eb6

Kroupa, P. 2001, MNRAS, 322, 231, doi: 10.1046/j.1365-8711.2001.04022.x

Linial, I., & Metzger, B. D. 2023, ApJ, 957, 34, doi: 10.3847/1538-4357/acf65b

—. 2024, arXiv e-prints, arXiv:2404.12421, doi: 10.48550/arXiv.2404.12421

Linial, I., & Sari, R. 2023, ApJ, 945, 86, doi: 10.3847/1538-4357/acbd3d

Liu, Z., Malyali, A., Krumpe, M., et al. 2023, A&A, 669, A75, doi: 10.1051/0004-6361/202244805

López-Cobá, C., Sánchez, S. F., Anderson, J. P., et al. 2020, AJ, 159, 167, doi: 10.3847/1538-3881/ab7848

Lops, G., Izquierdo-Villalba, D., Colpi, M., et al. 2023, MNRAS, 519, 5962, doi: 10.1093/mnras/stad058

Lu, W., & Quataert, E. 2023, MNRAS, 524, 6247, doi: 10.1093/mnras/stad2203

Metzger, B. D., Stone, N. C., & Gilbaum, S. 2022, ApJ, 926, 101, doi: 10.3847/1538-4357/ac3ee1

Miniutti, G., Giustini, M., Arcodia, R., et al. 2023, A&A, 670, A93, doi: 10.1051/0004-6361/202244512

Miniutti, G., Saxton, R. D., Giustini, M., et al. 2019, Nature, 573, 381, doi: 10.1038/s41586-019-1556-x

Pan, X., Li, S.-L., & Cao, X. 2023, ApJ, 952, 32, doi: 10.3847/1538-4357/acd180

Patra, K. C., Lu, W., Ma, Y., et al. 2024, MNRAS, doi: 10.1093/mnras/stae1146

Pawlik, M. M., Wild, V., Walcher, C. J., et al. 2016, MNRAS, 456, 3032, doi: 10.1093/mnras/stv2878

Payne, A. V., Shappee, B. J., Hinkle, J. T., et al. 2021, ApJ, 910, 125, doi: 10.3847/1538-4357/abe38d

Ponti, G., Papadakis, I., Bianchi, S., et al. 2012, A&A, 542, A83, doi: 10.1051/0004-6361/201118326

Quintin, E., Webb, N. A., Guillot, S., et al. 2023, A&A, 675, A152, doi: 10.1051/0004-6361/202346440

Raj, A., & Nixon, C. J. 2021, ApJ, 909, 82, doi: 10.3847/1538-4357/abdc25

Saxton, R., Read, A., Esquej, P., Miniutti, G., & Alvarez, E. 2011, arXiv e-prints, arXiv:1106.3507. https://arxiv.org/abs/1106.3507

Schawinski, K., Koss, M., Berney, S., & Sartori, L. F. 2015, MNRAS, 451, 2517, doi: 10.1093/mnras/stv1136

Schlafly, E. F., & Finkbeiner, D. P. 2011, ApJ, 737, 103, doi: 10.1088/0004-637X/737/2/103

Schweizer, F., Seitzer, P., Kelson, D. D., Villanueva, E. V., & Walth, G. L. 2013, ApJ, 773, 148, doi: 10.1088/0004-637X/773/2/148

Sheng, Z., Wang, T., Ferland, G., et al. 2021, ApJL, 920, L25, doi: 10.3847/2041-8213/ac2251

Sniegowska, M., Czerny, B., Bon, E., & Bon, N. 2020, A&A, 641, A167, doi: 10.1051/0004-6361/202038575

Tagawa, H., & Haiman, Z. 2023, MNRAS, 526, 69, doi: 10.1093/mnras/stad2616

Vazdekis, A., Coelho, P., Cassisi, S., et al. 2015, MNRAS, 449, 1177, doi: 10.1093/mnras/stv151

Wang, M., Ma, Y., Wu, Q., & Jiang, N. 2024, ApJ, 960, 69, doi: 10.3847/1538-4357/ad0bfb

Weaver, J., Husemann, B., Kuntschner, H., et al. 2018, A&A, 614, A32, doi: 10.1051/0004-6361/201732448

Wevers, T., Pasham, D. R., Jalan, P., Rakshit, S., & Arcodia, R. 2022, A&A, 659, L2, doi: 10.1051/0004-6361/202243143

Wevers, T., Coughlin, E. R., Pasham, D. R., et al. 2023, ApJL, 942, L33, doi: 10.3847/2041-8213/ac9f36

Wild, V., Heckman, T., & Charlot, S. 2010, MNRAS, 405, 933, doi: 10.1111/j.1365-2966.2010.16536.x

Zabludoff, A. I., Zaritsky, D., Lin, H., et al. 1996, ApJ, 466, 104, doi: 10.1086/177495

Zhao, Z. Y., Wang, Y. Y., Zou, Y. C., Wang, F. Y., & Dai, Z. G. 2022, A&A, 661, A55, doi: 10.1051/0004-6361/202142519

Zhou, C., Zhong, B., Zeng, Y., Huang, L., & Pan, Z. 2024, arXiv e-prints, arXiv:2405.06429, doi: 10.48550/arXiv.2405.06429